

MOL #100917

## **Long-range inhibitor-induced conformational regulation of human IRE1 $\alpha$ endoribonuclease activity**

Nestor O. Concha, Angela Smallwood, William Bonnette, Rachel Totoritis, Guofeng Zhang, Kelly Federowicz, Jingsong Yang, Hongwei Qi, Stephanie Chen, Nino Campobasso, Anthony E. Choudhry, Leanna E. Shuster, Karen A. Evans, Jeff Ralph, Sharon Sweitzer, Dirk A. Heerding, Carolyn A. Buser, Dai-Shi Su, & M. Phillip DeYoung

Oncology R&D (K.F., J.Y., L.E.S., K.A.E., J.R., D.A.H., C.A.B., D.S.S, M.P.D.), Biological Sciences (R.T., G.Z., H.Q., S.C., A.E.C., S.S.), and Chemical Sciences (N.O.C., A.S., W.B., N.C.), GlaxoSmithKline Research and Development, Collegeville, PA

MOL #100917

**Running Title:** Structure of human phosphorylated (active) IRE1 $\alpha$  dimer

**Corresponding author:**

M. Phillip DeYoung ([maurice.p.deyoung@gsk.com](mailto:maurice.p.deyoung@gsk.com)) or Nestor O. Concha

([Nestor.O.Concha@gsk.com](mailto:Nestor.O.Concha@gsk.com))

GlaxoSmithKline, Oncology R&D

1250 S. Collegeville Road, UP1450

Collegeville, PA 19426, USA

Phone : 610-917-5025

**Pages: 40**

**Tables: 1**

**Figures: 5**

**References: 46**

**Words in abstract: 244**

**Words in Introduction (including references and PDB IDs): 794**

**Words in Discussion (including references and PDB IDs): 1649**

**Non-standard abbreviations:**

APY29: 2-N-(3H-benzimidazol-5-yl)-4-N-(5-cyclopropyl-1H-pyrazol-3-yl)pyrimidine-2,4-diamine, ATF6: activating transcription factor 6, BIIC: baculovirus-infected insect cells, ER: endoplasmic reticulum, ERAD: ER-associated protein degradation, FP: fluorescence polarization, GSK2850163: (R)-2-(3,4-dichlorobenzyl)-N-(4-methylbenzyl)-2,7-diazaspiro[4.5]decane-7-carboxamide, HDX: hydrogen-deuterium exchange, IRE1 $\alpha$ : inositol-requiring enzyme-1 alpha, KIRA6: 1-(4-(8-Amino-3-tert-butylimidazo[1,5-a]pyrazin-1-yl)naphthalen-1-yl)-3-(3-(trifluoromethyl)phenyl)urea, PERK: PKR-like ER kinase, RIDD:

MOL #100917

regulated IRE1 $\alpha$  dependent degradation, RNase: endoribonuclease, SAR: structure activity relationship, STS: staurosporine, TEV: tobacco etch virus, UPR: unfolded protein response, UPRE: unfolded protein response element

MOL #100917

## ABSTRACT

Activation of the inositol-requiring enzyme-1 alpha (IRE1 $\alpha$ ) protein caused by endoplasmic reticulum (ER) stress results in the homodimerization of the N-terminal ER luminal domains, autophosphorylation of the cytoplasmic kinase domains, and conformational changes to the cytoplasmic endoribonuclease (RNase) domains which render them functional and can lead to the splicing of XBP1 mRNA. Herein we report the first crystal structures of the cytoplasmic portion of a human phosphorylated IRE1 $\alpha$  dimer in complex with GSK2850163, a novel, IRE1 $\alpha$ -selective kinase inhibitor, and with staurosporine (STS), a broad spectrum kinase inhibitor. GSK2850163 inhibits both the kinase and RNase activities of IRE1 $\alpha$ . The inhibitor interacts with the catalytic residues Lys599 and Glu612 and displaces the kinase activation loop to the DFG-out conformation. Inactivation of IRE1 $\alpha$  RNase activity appears to be caused by a conformational change whereby the  $\alpha$ C helix is displaced resulting in the rearrangement of the kinase domain-dimer interface and a rotation of the RNase domains away from each other. In contrast, STS binds at the ATP-binding site of IRE1 $\alpha$  resulting in a dimer consistent with RNase active yeast Ire1 dimers. Activation of IRE1 $\alpha$  RNase activity appears to be promoted by a network of hydrogen bond interactions between highly conserved residues across the RNase dimer interface that place key catalytic residues poised for reaction. These data implicate that the intermolecular interactions between conserved residues in the RNase domain are required for activity, and that the disruption of these interactions can be achieved pharmacologically by small molecule kinase domain inhibitors.

MOL #100917

## INTRODUCTION

Cellular stresses such as accumulation of unfolded proteins, hypoxia, glucose deprivation, depletion of ER calcium levels, and changes in ER redox status activate the unfolded protein response (UPR), an intracellular signal transduction network involved in restoring protein homeostasis (reviewed in Walter and Ron, 2011). To alleviate these types of stress responses, the UPR responds by halting protein translation, activating transcription of UPR-associated target genes, and degrading misfolded proteins (Ron, 2002; Harding, et al, 2002; Feldman et al., 2005). UPR signaling also regulates cell survival by modulating apoptosis and autophagy and can induce cell death under prolonged ER stress if the misfolded protein burden is too high (Woehlbier and Hetz, 2011; Ma and Hendershot, 2004; Rouschop et al., 2010).

Three key ER membrane proteins have been identified as primary effectors of the UPR: PKR-like ER kinase (PERK), inositol-requiring enzyme 1  $\alpha/\beta$  (IRE1), and activating transcription factor 6 (ATF6) (Schroder and Kaufman, 2005). IRE1 $\alpha$  is a transmembrane protein that functions both as an ER stress sensing receptor via its N-terminal ER luminal domain and as a signal transducer via its cytoplasmic C-terminal kinase and RNase domains (Tirasophon et al., 1998). Upon sensing ER stress, the extracellular portion of the IRE1 $\alpha$  protein will homodimerize, allowing for trans autophosphorylation, which, in turn, induces a conformational change resulting in activation of the RNase domains (Ali et al., 2011). Phosphorylation within the kinase activation loop is an essential step for RNase activation (Prischi et al., 2014). Mammalian IRE1 $\alpha$  excises a 26-bp intron from the mRNA of XBP1 that causes a translational frame shift downstream of the splice site to produce XBP1s, the active form of the transcription factor (Yoshida et al., 2001; Calton et al., 2002; Lee et al., 2002). XBP1 is responsible for the

MOL #100917

activation of key UPR target genes, including molecular chaperones and components of the ER-associated protein degradation (ERAD) machinery (Lee et al., 2003). Activation of IRE1 $\alpha$  is also reported to result in the induction of regulated IRE1 $\alpha$  dependent degradation (RIDD) of a subset of mRNAs encoding secretory proteins or the induction of apoptosis via IRE1 $\alpha$  signaling through its kinase domain and downstream effectors ASK1, JNK1, and Caspase-12 (Hollien and Weissman, 2006; Urano et al., 2000).

Loss of ER homeostasis (i.e., loss or hyperactivation of UPR signaling) has been attributed to a number of diseases, including cancer, diabetes, cardiovascular diseases, liver diseases, and neurodegenerative disorders, and the UPR is increasingly becoming an attractive pathway in drug discovery (Hetz et al., 2013; Maly and Papa, 2014). To this end, an increasing body of work has been performed to identify potent and selective molecules of IRE1 $\alpha$  and to better understand how these molecules bind and affect IRE1 $\alpha$  activation mechanisms. Crystal structures of the C-terminal region of phosphorylated (active) yeast Ire1 were the first to be characterized and revealed that Ire1 forms dimers arranged in a “back-to-back” configuration with the kinase active sites facing outward (PDB ID [2RIO](#); Lee et al., 2008; PDB ID [3FBV](#); Korennykh et al., 2009; PDB ID [3LJ0](#); Wiseman et al., 2010). This dimer arrangement also formed the basis of a rod-shaped helical structure representing a high-order oligomeric Ire1 structure in complex with the kinase inhibitor APY29 ([3FBV](#); Korennykh et al., 2009). These yeast “back-to-back” structures contrast with the first reported human IRE1 $\alpha$  dimer: a dephosphorylated C-terminal IRE1 $\alpha$ -Mg<sup>2+</sup>-ADP complex possibly representing an early state prior to phosphoryl-transfer (PDB ID [3P23](#); Ali et al., 2011). In this structure, the kinase active sites are facing each other and are in a suitable orientation and proximity for trans autophosphorylation, but the RNase domains are far from each other and inactive. A similar

MOL #100917

“face-to-face” structure was recently reported for mouse IRE1 $\alpha$ , but this structure was phosphorylated (PDB ID [4PL3](#); Sanches et al., 2014). More recently, a few other dephosphorylated human crystal structures were reported. One is of a co-crystal structure containing a kinase domain inhibitor bound to an IRE1 $\alpha$  monomer (PDB ID [4U6R](#); Harrington et al., 2014). Here, no dimers were found with the inhibitor-bound structure suggesting that the compound may either prevent dimerization or stabilize a monomeric IRE1 $\alpha$ . The second report presented two “back-to-back” dimers of IRE1 $\alpha$ , one in apo form and one in an inhibitor-bound form (PDB IDs [4Z7G](#) and [4Z7H](#); Joshi et al., 2015). These structures are consistent with yeast Ire1 dimers but are distinct in that the apo structure contains a twisted interface between the dimers across the RNase domains which may represent an additional intermediate of IRE1 $\alpha$  prior to full activation. The culmination of all these structures may depict the IRE1 protein at various levels of activation and suggest that this process is conserved evolutionarily. Here we present a proposed structure of the final state of a human phosphorylated (active) IRE1 $\alpha$  dimer co-crystallized with two kinase inhibitors that have opposing effects to the RNase activity of the protein.

MOL #100917

## MATERIALS AND METHODS

### IRE1 $\alpha$ protein expression and purification

The cytosolic domain of human IRE1 $\alpha$  (NM\_001433) encompassing amino acids 547-977 was cloned into pENTR/TEV/D-TOPO (Life Technologies, Carlsbad, CA) and subsequently transferred to a pDest8 (Life Technologies) vector backbone containing N-terminal Flag epitope tag followed by 6xHis tag and tobacco etch virus (TEV) cleavage site (ENLYFQG/S). Baculovirus generation was accomplished using the Bac-to-Bac<sup>®</sup> baculovirus generation system (Life Technologies). Flag-His<sub>6</sub>-TEV-IRE1 $\alpha$  (547-977) protein expression in baculovirus-infected insect cells (BIIC) was accomplished following established procedures (Wasilko and Lee, 2006). Briefly, a proprietary Sf9 insect cell line was grown to early log phase, infected with 1x10<sup>7</sup> BIIC/10 L culture and incubated at 27°C. Cell paste was harvested at 66-72 h post infection. Human phosphorylated or dephosphorylated IRE1 $\alpha$  protein containing N-terminal Flag-His<sub>6</sub> tags and a TEV protease cleavage site between the tags and IRE1 $\alpha$  protein was purified from ~150 g of cells from a 10L culture (lysed in 1.5 L lysis buffer (50 mM Hepes, pH 7.5, 10% glycerol, 300 mM NaCl) by EmulsiFlex-C50 homogenizer (Avestin, Ottawa, ON). The protein in the clear supernatant from centrifugation at 30,000g for 30 min at 4°C was first captured in 20 ml NiNTA-SF beads (Qiagen, Venlo, Netherlands) in batch mode for 4 h at 4°C. The beads were poured into a column, washed with 20 mM imidazole in lysis buffer, and the IRE1 $\alpha$  protein was eluted from the column by 300 mM imidazole in 50 mM Hepes, pH 7.5, 150 mM NaCl buffer. The Ni elution pool was concentrated using a 10 kDa MW cutoff filter concentrator to about 25 ml to which 3 mg of Tev protease was added to remove the His<sub>6</sub> tag. This mixture was then transferred into dialysis tubing (8 kDa MW cutoff) and dialyzed overnight against 3L MonoQ buffer A (50 mM Hepes, pH 7.5, 50 mM NaCl, 5 mM DTT, 1 mM EDTA),



MOL #100917

passed through a second 20 ml Mono Q column (GE Healthcare, Piscataway, NJ), and eluted with a 50-500 mM NaCl gradient over 10 column volumes. The eluted samples were analyzed by LC-MS, and the major peak with a mass consistent with the expected molecular weight for the protein plus three phosphates (80 mass units per phosphate) was purified in a Hiload Superdex 200 sizing column (GE Healthcare) with a buffer of 50 mM Hepes, pH 7.5, 200 mM NaCl, 5 mM DTT, 1 mM EDTA. The eluted protein (2-3 mg protein in 1 ml aliquots) was stored at -80°C and later used in assays and crystallography. The remaining fractions from the Mono Q column were pooled and treated with  $\lambda$ -phosphatase to produce the fully dephosphorylated enzyme before it was further purified and stored in the same way as the triply phosphorylated protein.

### **pIRE1 $\alpha$ RNase activity assay**

The nuclease enzymatic activity of phosphorylated IRE1 $\alpha$  (pIRE1 $\alpha$ ) was measured using a dual labeled 36-mer RNA substrate that contained the IRE1 $\alpha$  recognition sequence with a 6-carboxyfluorescein fluorescent reporter (6-FAM) at the 3' end, and the Black Hole quencher -1 (BHQ-1) at the 5' end (5'/6-FAM/rCrArG rUrCrC rGrCrA rGrCrA rCrUrG/BHQ-1/3'; Integrated DNA Technologies, Coralville, IA). Upon cleavage, the release of FAM results in an increase in fluorescent signal measured at  $\lambda_{ex}/\lambda_{em} = 485/535\text{nm}$ . A typical enzymatic reaction was carried out with 10 nM pIRE1 $\alpha$  and 500 nM substrate in a buffer containing 20 mM HEPES, pH 7.5, 5 mM MgCl<sub>2</sub>, 10 mM NaCl, 1 mM DTT, 0.05% Tween-20 and 0.02% heat-treated casein (heated for 20 min at 60°C prior to use each time), and the fluorescence change was followed using an Envision plate reader (PerkinElmer, Waltham, MA).

MOL #100917

To identify inhibitors of IRE1 $\alpha$  nuclease activity, pIRE1 $\alpha$  was screened against the GSK compound collection. The RNA oligomer substrate was added to the assay plates containing 10  $\mu$ M compound. The reaction was initiated immediately by the addition of enzyme and the plates centrifuged for 1 minute at 500 rpm. The final reaction mixture contained 10 nM pIRE1 $\alpha$ , 25 nM RNA oligomer, 20 mM HEPES pH 7.5, 5 mM MgCl<sub>2</sub>, 1 mM DTT, 0.05% Tween-20, 10 mM NaCl, and 0.02% casein. The reaction plates were incubated at room temperature for 90 minutes before the reaction was terminated with 0.015% SDS in 20 mM HEPES, pH 7.5. The plates were centrifuged for 3 min at 1000 rpm prior to measuring product formation using the Viewlux imager (PerkinElmer).

### **pIRE1 $\alpha$ kinase assays**

In the ADP-Glo<sup>TM</sup> assay, a compound's potency towards pIRE1 $\alpha$  kinase activity was measured as its inhibition of an intrinsic, slow ATP hydrolysis activity. 100 nL DMSO solution of GSK2850163, at various concentrations, was added into a white Greiner low volume 384 well plate. The reaction was carried out with 5 nM pIRE1 $\alpha$  and 60  $\mu$ M ATP in 10  $\mu$ L 50 mM HEPES buffer, pH 7.5, containing 30 mM NaCl, 10 mM MgCl<sub>2</sub>, 1 mM DTT, 0.02% Chaps and 0.01 mg/mL BSA. The reaction was stopped after 2 h by adding 5  $\mu$ L ADP-Glo<sup>TM</sup> reagent I, which also depletes the remaining ATP. Following a 1 h incubation, 5  $\mu$ L ADP-Glo<sup>TM</sup> reagent II was added into the reaction, which converts the ADP product into ATP to serve as substrate for the coupled luciferin/luciferase reaction. After 30 min, the plate was read on a Wallac ViewLux microplate imager.

In the fluorescence polarization (FP) assay, a compound's affinity was measured by its ability to compete with a fluorescent labeled ATP site ligand for binding to the kinase domain.

MOL #100917

The FP assay was carried out in the same reaction buffer described above. A 10  $\mu$ L reaction contained 5 nM IRE1, 5 nM fluorescent ligand (GSK369716A), and GSK2851063 at various concentrations. After the addition of reagents, the plate was incubated at room temperature for 15 min and then read on an Analyst GT multimode reader (Molecular Devices, Sunnyvale CA) at excitation/emission of 485nm/530nm with a dichroic of 505 nm. IC<sub>50</sub> values were calculated using the data fitting software GraFit (Erithacus Software).

### **PERK kinase assay**

Recombinant PERK protein (Life Technologies) was purchased for use in a selectivity assay to test pIRE1 $\alpha$  inhibitors. Solution of PERK (0.40 nM) in assay buffer containing 10 mM HEPES, pH 7.5, 2 mM CHAPS, 5 mM MgCl<sub>2</sub>, and 1 mM DTT was pre-incubated with compound for 30 min at room temperature. The reaction was initiated by the addition of substrate mix which contained 0.040  $\mu$ M biotinylated eIF2 $\alpha$  (eukaryotic translation initiation factor 2 $\alpha$ ) peptide and 5  $\mu$ M ATP. The reaction plates were incubated at room temperature for 60 min, followed by termination with a detection/quench mixture. The detection/quench mixture contained 15 mM EDTA, 4 nM eIF2 $\alpha$  phospho antibody (Millipore, Billerica, MA), 4 nM europium-labeled anti-rabbit antibody (PerkinElmer) and 40 nM streptavidin APC (PerkinElmer). The plates were incubated for 10 min at room temperature prior to measuring HTRF signal (excitation at 610-640nm, emission at 660nm) using the Viewlux imager.

### **RNase L activity assay**

A solution of 0.1 nM RNase L, 1  $\mu$ M ATP, and 8 nM 2-5A (2',5'-linked oligoadenylate, p<sub>1-3</sub>(A<sub>2</sub>'p5'A)<sub>n $\geq$ 2</sub>) in assay buffer containing 20 mM HEPES, pH 7.5, 10 mM MgCl<sub>2</sub>, 1 mM TCEP, 0.5 mM CHAPS, 100 mM NaCl, and 0.02% casein was incubated at room temperature

MOL #100917

for 30 minutes. A 0.2  $\mu$ M solution of a 36-mer RNA substrate (5'/6-FAM rUrUrA rUrCrA rArArU rUrCrU rUrArU rUrUrG rCrCrC rCrArU rUrUrU rUrUrU rGrGrU rUrUrA BHQ-1/3'; Integrated DNA Technologies) was prepared in assay buffer and added to reaction plates containing compounds. The reaction was initiated with the addition of RNase L-ATP-2-5A mixture and the plates incubated at room temperature for 90 min. Following the incubation, the reaction was terminated with 0.02% SDS solution in nuclease free water. The plates were centrifuged for 3 min at 1000 rpm prior to measuring product formation using the Viewlux imager.

### **Competitive inhibition studies**

In single compound inhibition studies, the concentrations of the substrate or non-cleavable substrate (analog in which the ribose linked to the guanine at the cleavage site was replaced by deoxyribose), and GSK2850163 were varied and the enzyme concentration was fixed at 10 nM. The modes of inhibition and the inhibition constants were determined by fitting the initial velocities to different models (competitive, uncompetitive and noncompetitive) using Grafit software. In a double inhibition experiment, the concentration of the first inhibitor was varied at several different concentrations of the second inhibitor, and the concentrations of the enzyme and substrate were kept constant at 10 nM and 100 nM, respectively. The reactions were monitored kinetically and the initial reaction velocities were analyzed using the Yonetani-Theorell equation.

### **Protein crystallization and structure determination**

Crystals of pIRE1 $\alpha$  (547-977) with GSK2850163 (PDB: 4YZ9) were prepared by mixing pIRE1 $\alpha$  with 0.5 mM GSK2850163 and incubating overnight on ice. The crystals were grown at

MOL #100917

20°C by vapor diffusion in sitting drops containing 2 µl of protein (13 mg/ml in 50 mM Hepes, pH 7.5, 200 mM NaCl, 5 mM DTT, 1 mM EDTA, 0.5 mM GSK2850163, 0.25% DMSO) and 2 µl reservoir solution containing PEG 3350 (16%-22%), 100 mM Hepes pH 7.0, 200 mM Ca<sup>2+</sup> acetate. The crystals were thick rods that appeared over 2-5 days and reached full size (0.05 X 0.025 X 0.3 mm) in 2 weeks. Seeding was used to improve crystal quality. The pIRE1α + GSK2850163 crystals were frozen in a solution of 20% ethylene glycol, 22% PEG 3350, 0.2 M calcium acetate added in a stepwise manner to the protein drop before mounting the crystal on the loop.

The crystals of pIRE1α with Mg<sup>2+</sup>-ADP (PDB: 4YZD) were grown by mixing 2 µl protein solution (10 mg/ml pIRE1α (547-977) in 50 mM Hepes, pH 7.5, 200 mM NaCl, 5 mM DTT, 1 mM EDTA, 1 mM ADP (100 mM ADP stock was ~ pH 7.0), 1 mM MgCl<sub>2</sub>) with 2 µl reservoir solution (16 % PEG 3350, 200 mM Na<sup>+</sup> Malonate pH 6.0) in sitting drops at room temperature. Seeding was used to initiate crystal growth. Crystals appeared the next day and grew to full size in 3 weeks. For data collection, the crystals were frozen in a solution of 20% ethylene glycol, 22% PEG 3350, 200 mM Na<sup>+</sup> Malonate pH 6.0 and added to the protein drop before mounting the crystals on the loop.

The complex of pIRE1α (547-977) with staurosporine (PDB: 4YZC) was prepared by mixing the protein with 0.5 mM staurosporine and incubated overnight on ice. The crystals were grown at 20°C by vapor diffusion in sitting drop containing 2 µl of protein (13 mg/ml in 50 mM Hepes, pH 7.5, 200 mM NaCl, 5 mM DTT, 1 mM EDTA) and 2µl reservoir solution containing PEG 300 (30%-40%), 100 mM Hepes pH 7.5, 200 mM KCl. Small hexagonal plates appeared over 5-10 days and reached full size (0.05 X 0.75 X 0.15 mm) in ~20 days. The crystals were

MOL #100917

flash-frozen in liquid N<sub>2</sub> directly from the crystallization drop. All diffraction data was collected at the Advanced Photon Source, Argonne National Laboratories, Life Sciences CAT, Sector 21.

All structures were determined by molecular replacement with Phaser (Afonine et al., 2010) as implemented in CCP4 (Winn et al., 2011) using the human dephosphorylated IRE1 $\alpha$ -Mg<sup>2+</sup>-ADP complex (3P23; Ali et al., 2011) as a model. Refinement was performed by a combination of Refmac5 (Murshudov et al., 1997) and Phenix (Afonine et al., 2010) with manual adjustments to the model in COOT (Emsley and Cowtan, 2004). The quality of the model was monitored using Molprobit (Chen et al., 2010). Figures were made with PYMOL (Schrödinger, LLC, New York, NY).

### **Detection of XBP1 splicing by RT-PCR**

Multiple myeloma cancer cell lines were obtained from ATCC (Manassas, VA) or DSMZ (Braunschweig, Germany). Cells were cultured in the appropriate culture medium supplemented with 10% FBS (Sigma-Aldrich, St. Louis, MO) at 37°C in humidified incubators under 5% CO<sub>2</sub>. Cells were seeded into 6-well plates at a density of 1.5x10<sup>6</sup> cells/well in the appropriate media containing 1% FBS media and were treated with 5  $\mu$ g/mL tunicamycin (MP Biomedicals, Newport Beach, CA) for 1 h before the addition of GSK2850163 for 3 h (four hours total). For studies involving staurosporine (Sigma-Aldrich) treatment, cells were treated with staurosporine for 30 min followed by 5  $\mu$ g/mL tunicamycin for 1 h. RNA was collected using the Qiagen RNEasy Mini Kit. RNA was quantitated using a NanoDrop (Thermo Scientific, Philadelphia, PA) and stored at -80°C. To generate cDNA, the High-Capacity cDNA Reverse Transcription Kit (Life Technologies) was used. For PCR, a 25  $\mu$ L reaction included 12.5  $\mu$ L of Master Mix (Promega Go-Taq 2X Master Mix), 1  $\mu$ L each of forward and reverse primers (100 ng/ $\mu$ L), 9.5

MOL #100917

$\mu\text{L}$  of water, and 1  $\mu\text{L}$  of cDNA template. Primers for human XBP1 were: Forward: 5'-CCTGGTTGCTGAAGAGGAGG-3' and Reverse: 5'-CCATGGGGAGATGTTCTGGG-3'. RT-PCR conditions were: 95°C for 5 min; 95°C for 30 sec; 58°C for 30 sec; 72°C for 30 sec; 72°C for 5 min with 35 cycles of amplification. After RT-PCR, reactions were run on a 3% agarose gel and visualized using SYBR<sup>®</sup> Safe DNA gel stain (Life Technologies) and a BioRad Imager (Hercules, CA).

### **Western blot analysis**

RPMI 8226 cells were seeded into 6-well plates at a density of  $2.0 \times 10^6$  cells/well in RPMI 1640 media containing 1% FBS. Cells were treated with the same conditions as described above for XBP1 splicing detection by RT-PCR. To harvest protein lysates, cells were lysed with 60  $\mu\text{L}$  of 1X cell lysis buffer (Cell Signaling Technologies, Danvers, MA) containing protease and phosphatase inhibitors. Cell lysates were quantified using the Pierce BCA Protein Assay Kit (Thermo Scientific) and samples were read on a SPECTRAmax 190 instrument. Following quantitation, 40  $\mu\text{g}$  of protein was run on 4-12% Bis-Tris gels (LifeTechnologies), and protein was transferred onto 0.45  $\mu\text{M}$  nitrocellulose membranes (LifeTechnologies) using the BioRad semi-dry transfer blotting apparatus. Membranes were blocked for one hour using Li-Cor Odyssey Blocking Buffer then probed with the following antibodies overnight: pIRE1 $\alpha$  S724 (Abcam, #ab48187; 1:1000), total IRE1 $\alpha$  (Abcam, #ab37073; 1:1000), and GAPDH (Bethyl Laboratories, #A300-639A; 1:2000). After washing, blots were incubated with donkey anti-rabbit IRDye-800CW secondary antibody (Li-Cor), and proteins were visualized using the Odyssey Imaging System.

MOL #100917

### **XBP1 transcriptional activity assay**

PANC-1 cells were seeded into 6-well plates at a density of  $5.0 \times 10^3$  cells/well in RPMI 1640 media containing 10% FBS. Cells were co-transfected with a pGL3-5xUPRE-luciferase reporter containing five repetitions of the XBP-1 DNA binding site (a kind gift from R. Prywes, Columbia University) and pRL-SV40 (Promega, Madison, WI) using FuGENE6 transfection reagent (Roche, Indianapolis, IN). Forty eight hours later, cells were treated with 2.5  $\mu\text{g}/\text{mL}$  tunicamycin for 1 hour followed by GSK2850163 treatment for 16 hours. Luciferase expression was measured using Dual-Glo Luciferase Assay kit (Promega) and normalized to renilla expression levels.

### **Hydrogen-Deuterium Exchange**

pIRE1 $\alpha$  (547-977, 78  $\mu\text{M}$ ) was incubated with 250  $\mu\text{M}$  GSK2850163 or 1 mM staurosporine for at least 18 hours. 2  $\mu\text{l}$  of protein-inhibitor mixture was mixed with 18  $\mu\text{l}$  D<sub>2</sub>O at room temperature for 1 minute, after which 20  $\mu\text{l}$  of 4M guanidinium chloride in 1M glycine buffer, pH 2.5 and 120  $\mu\text{l}$  formic acid were added and immediately transferred to an ice cold bath. All subsequent treatment and analysis was done at 2-4°C. 50  $\mu\text{l}$  of this solution was injected into a Waters Enzymate BEH pepsin 2.1 x 30 mm column for digestion, then to a C18 column and into a LTQ XL Orbitrap mass spectrometer. The z/m values were calculated with XCalibur and compared with sequences in the MASCOT database. The analysis of the H/D exchange was done with HDEaminer. Tryptic digestion of all the samples gave a sequence coverage of at least 98% of the amino acid sequence.

### **Preparation and characterization of compounds 1-24**



MOL #100917

Details provided in supplementary methods.

## RESULTS

### Crystallization of the novel inhibitor GSK2850163 bound to pIRE1 $\alpha$

Because of the relevance of the IRE1 $\alpha$ /XBP1 pathway in human disease, we sought to identify small molecules that would inhibit IRE1 $\alpha$  RNase activity. GSK2850163 was discovered as a result of a high-throughput screening campaign to identify IRE1 $\alpha$ -selective inhibitors of XBP1 splicing. It is a highly selective inhibitor with dual activity: it inhibits IRE1 $\alpha$  kinase activity ( $IC_{50} = 20$  nM) and RNase activity ( $IC_{50} = 200$  nM) (Fig. 1A, Supplementary Table 1). In competition kinetic studies, GSK2850163 and a noncleavable RNA substrate demonstrated mutually exclusive binding to activated IRE1 $\alpha$  ( $K_i = 200 \pm 20$  nM) (Supplementary Fig. 1). We hypothesized that this was due to bound GSK2850163 altering the preferred enzyme structure for RNA substrate binding (and vice versa) and not due to a physical overlapping of binding sites.

To investigate the mode of binding and to enable structure-guided optimization of GSK2850163, we determined the co-crystal structure of GSK2850163 with the C-terminal portion of the phosphorylated human IRE1 $\alpha$  protein (pIRE1 $\alpha$ , residues 547-977, PDB ID: 4YZ9) (Fig. 1B, Supplementary Fig. 2, Table 1). The structure of pIRE1 $\alpha$ -GSK2850163 is of a “back-to-back” dimer with one inhibitor molecule bound to the kinase domain of each protomer in a pocket next to the kinase  $\alpha$ C helix, approximately 12 Å from hinge region (Fig. 1C). GSK2850163 adopts a “U” shaped conformation with the tolyl and dichlorophenyl groups facing the inside of the protein and the spirodecane core partially solvent exposed with the piperidine ring (A-ring) in a chair conformation. Two key interactions with conserved kinase catalytic residues, Glu612 and Lys599, are observed. The urea nitrogen and the pyrrolidine nitrogen of

MOL #100917

GSK2850163 form a hydrogen bond interaction with the side chain of Glu612, and the carbonyl oxygen of the urea of GSK2850163 interacts through a hydrogen bond with the side chain of Lys599.

GSK2850163 displaces the kinase activation loop of pIRE1 $\alpha$  such that the DFG motif is in the “out” conformation and is flipped by nearly 180° occupying the ATP binding site (Fig. 1C). This clearly contrasts with our resolved structure of pIRE1 $\alpha$ -ADP-Mg<sup>2+</sup> (PDB ID: 4YZD) where the DFG motif is found in the “in” conformation and Phe712 occupies the same pocket where the GSK2850163 binds in the pIRE1 $\alpha$ -GSK2850163 structure (Fig. 1D and Table 1). Phe712 makes a  $\pi$  interaction with Tyr628 in a pocket lined by Val613, Leu616, Val625, and Leu679. Superposition of the ADP-Mg<sup>2+</sup> and GSK2850163-bound pIRE1 $\alpha$  complexes shows that GSK2850163 does not overlap with the ATP-binding site (data not shown). The structure of pIRE1 $\alpha$  in complex with Mg<sup>2+</sup>-ADP forms a “face-to-face” dimer across the symmetry planes with neighboring molecules (Supplementary Fig.3). Consistent with previously published structures, the kinase active sites are facing each other and are in an orientation and proximity favorable for trans autophosphorylation (3P23; Ali et al., 2011; 4PL3; Sanches et al., 2014). The present structure may possibly represent an early post-phosphoryl-transfer dimer, while the “face-to-face” structure of dephosphorylated human IRE1 $\alpha$  may represent a state just prior to phosphoryl-transfer.

### **Structure activity relationship of GSK2850163**

To provide supportive evidence for the binding mode of GSK2850163 observed in the crystal structure, we performed structure activity relationship (SAR) studies whereby we systematically modified the structure of the ligand and followed the effect by measuring pIRE1 $\alpha$

MOL #100917

RNase inhibition. First, we observed that while the *S*-enantiomer is inactive and its conformation does not fit in the electron density map, the *R*-enantiomer inhibited the RNase activity *in vitro* with an  $IC_{50} = 0.2 \mu\text{M}$  (Fig. 2A). The *R*-enantiomer is refined in the structure of the complex. Since the activity of the *R*-enantiomer is equally potent to the racemic compound and *S*-enantiomer is not active, the initial SAR study was performed with the racemic analogs.

Secondly, the NH of urea nitrogen and the pyrrolidine nitrogen are required to make a H-bond with Glu612 (2.98Å), and any changes in the GSK2850163 (compound **1**) molecule disrupting these specific H-bond interactions resulted in loss of activity. For example, replacement of the urea nitrogen (compound **2**) or capping the NH with a methyl group (compound **3**) caused a loss of potency (Fig. 2A). Similarly, conversion of a basic amine in pyrrolidine ring to a non basic amide yielded an inactive analog (compound **4**, Fig. 2A).

Thirdly, in the binding mode of GSK2850163 in complex with pIRE1 $\alpha$  described here, the lipophilic groups at both ends of molecule (the tolyl and dichlorophenyl groups) are accommodated within the lipophilic pockets observed in the core crystal structure (Supplementary Fig. 2B) and are critical for the inhibitor's activity. All analogs with polar functionality, such as pyridines, were not active (compounds **5-6**, Fig. 2B) or much less active (compounds **15-19**, Fig. 2C). On the other hand, the lipophilic groups were well tolerated (compounds **8-14**, **20-24**) in the hydrophobic pocket. Deletion of one of the chlorines to form 3- or 4-mono chloro analogs (**7** and **8**, respectively) revealed that the 4-chloro substitution was more tolerated than 3-position in term of potency (Fig. 2B). Replacement of 3-chloro with other groups, such as fluoro (**11**), methyl (**12**), or methoxy (**13**), provided equally potent analogs, but the trifluoromethyl group (**14**) caused a significant loss of potency. The tolyl group at the A-ring urea preferred lipophilic substitutions, and polar functionalities (*e.g.* pyridines (**15-17**) and

MOL #100917

substituted pyridines (**18-19**) were not tolerated. Deletion of the methyl group gave the simple phenyl analog **20** that maintained RNase activity ( $IC_{50} = 0.40 \mu M$ ) (Fig. 2B). Replacement of the methyl group at the 4-position with other lipophilic groups, such as, chlorine (**21**), methoxy (**22**), fluorine (**23**) was well tolerated. The benzodioxole analog **24** exhibited an  $IC_{50}$  value of 100 nM. These SAR study results are consistent with the binding mode of GSK2850163 to pIRE1 $\alpha$  observed in the crystal structure, and indicate that GSK2850163 functions as a kinase and RNase inhibitor of pIRE1 $\alpha$ .

### Cellular activity of GSK2850163

We utilized a panel of eight multiple myeloma cell lines to test the effects of GSK2850163 on IRE1 $\alpha$  RNase activity. Increased IRE1 $\alpha$  activity has been observed in primary multiple myeloma specimens, and clinical studies have associated high levels of spliced XBP1 mRNA with poor patient survival (Reimold et al., 2001; Nakamura et al., 2006; Bagratuni, et al., 2010). To recapitulate an ER stress-induced environment in cell culture, tunicamycin, an inhibitor of N-linked glycosylation, was used (Yoshida et al., 2001). XBP1 mRNA is found primarily in the unspliced form under basal conditions. Upon ER stress stimulation, all cells induced varying degrees of XBP1 splicing that could be reversed following treatment with GSK2850163 (Fig. 3A). ER stress also induced increased autophosphorylation of IRE1 $\alpha$ , which could be reduced in a dose-dependent manner by GSK2850163 (Fig. 3B). To determine if GSK2850163 could affect the transcriptional function of XBP1, cells expressing a reporter plasmid under the control of five tandem repeats of the Unfolded Protein Response Element (UPRE) motif were treated with tunicamycin followed by increasing doses of GSK2850163 (Wang et al., 2000). The UPRE sequence contains the binding site found at the promoter of

MOL #100917

XBP1 target genes. Induction of ER stress by tunicamycin significantly increases XBP1 transcriptional activity in these cells, yet increasing concentrations of GSK2850163 are capable of reducing this activity (Fig. 3C). These data support our biochemical and structural evidence that GSK2850163 is an inhibitor of IRE1 $\alpha$ , capable of inhibiting both kinase and RNase activities of IRE1 $\alpha$ .

### **Crystallization of staurosporine bound to pIRE1 $\alpha$**

To further understand the mechanism by which the RNase activity of IRE1 $\alpha$  could be modulated pharmacologically with kinase inhibitors, we sought to investigate the effect of the broad-spectrum kinase inhibitor staurosporine (STS) on IRE1 $\alpha$ . It has been previously shown that STS inhibits IRE1 $\alpha$  kinase activity (Ali et al., 2011) and is likely to bind to the ATP-binding site of IRE1 $\alpha$  since it competed with the irreversible IRE1 $\alpha$  inhibitor, 4 $\mu$ 8C, preventing the formation of a Schiff base with the kinase active site residue Lys599 (Cross et al., 2012). We found that STS inhibited pIRE1 $\alpha$  kinase enzymatic activity (IC<sub>50</sub>= 3 nM) but had no effect on pIRE1 $\alpha$  RNase activity *in vitro* (Fig. 4A). STS exhibited similar binding affinity towards phosphorylated IRE1 $\alpha$  (IC<sub>50</sub>= 30 nM) and dephosphorylated IRE1 $\alpha$  (IC<sub>50</sub>= 50 nM) in a competitive binding assay (data not shown). Interestingly, incubation of STS with dephosphorylated (inactive) IRE1 $\alpha$  was capable of activating IRE1 $\alpha$  RNase activity (Fig. 4B). To test the effects of STS on IRE1 $\alpha$  RNase activity in a cellular context, RPMI 8226 multiple myeloma cells were treated with STS followed by tunicamycin to measure XBP1 splicing. STS treatment alone was sufficient to induce XBP1 splicing, similar to levels achieved with tunicamycin (Fig. 4C). Despite inducing XBP1 splicing, STS did not increase IRE1 $\alpha$  autophosphorylation. Instead, STS inhibited tunicamycin-induced autophosphorylation (Fig.

MOL #100917

4D). STS treatment may also inhibit IRE1 $\alpha$  autophosphorylation below basal levels, but it was difficult to measure this convincingly by Western blot analysis. These observations, both biochemical and in cells, suggest that the effects of STS on IRE1 $\alpha$  phosphorylation and XBP1 splicing could be due to direct binding of STS to IRE1 $\alpha$  and not just due to general stress that could occur due to the broad-spectrum nature of the compound.

To understand the structural basis of the activation of the RNase activity of IRE1 $\alpha$  by staurosporine, we determined the crystal structure of the human pIRE1 $\alpha$ -STS complex (PDB ID: 4YZC, Table 1). The pIRE1 $\alpha$ -STS complex forms a back-to-back dimer with one STS molecule bound per protomer (Fig. 4E, Supplementary Fig. 4A). STS binds in the ATP-binding site of the kinase domain and interacts with hinge residues Glu643, Cys645, and His692 (Supplementary Fig. 4B). The activation loop containing phosphorylated Ser residues (pSer724, pSer726, and pSer729) that was previously disordered in both the pIRE1 $\alpha$ -GSK2850163 and the pIRE1 $\alpha$ -ADP complexes is well defined in the pIRE1 $\alpha$ -STS complex (Supplementary Fig. 4C). pSer724 interacts with Asn750 via two H-bonds, pSer726 is involved in a H-bond interaction with Arg722 (3.1 Å) and Arg728 (3.3 Å), and pS729 is interacting through a H-bond with Lys716 (2.7 Å) and Arg687 (2.5 Å). A network of H-bonds extends from the serines in the activation loop to the  $\alpha$ C helix and into the active site DFG motif. Binding of STS to pIRE1 $\alpha$  locks the kinase domain in a conformation in which the (i) activation loop is in the DFG (711-713)-in conformation; (ii) the DFG-aspartate interacts with His689 in the HRD motif in the catalytic loop; (iii) the conserved Leu616 in the  $\alpha$ C helix interacts with the DFG-phenylalanine in the regulatory spine of the kinase; and (iv) Arg687 of the HRD motif interacts with pSer729 (Supplementary Fig. 4C). These are the signatures of a kinase in the active conformation

MOL #100917

(Kornev and Taylor, 2010). Attempts to crystallize dephosphorylated IRE1 $\alpha$  with STS were not successful.

### **Comparison of pIRE1 $\alpha$ dimer interactions and protein dynamics**

To test the pIRE1 $\alpha$  dimer interactions observed in the structures, we determined the hydrogen-deuterium exchange of pIRE1 $\alpha$  in the presence or absence of either GSK2850163 or STS in solution (Supplementary Fig. 5). Changes in the labeling pattern can be related to changes in protein structure or dynamics resulting from a ligand binding event (Percy et al., 2012; Englander et al., 2003). By mapping the observed labeling onto the two co-crystal structures, we observed three areas where most of the structural changes occurred. The first region is in the vicinity of the ligand binding site (Supplementary Fig. 6A). Increased solvent exposure of the activation loop and the disruption of the conserved salt bridge Arg627 - Asp620 by GSK2850163 are both consistent with the displacement of the activation loop to the DFG-out conformation, and the changes in the  $\alpha$ C helix to the inactive conformation (Supplementary Fig. 6B). Secondly, in the presence of STS the residues at the kinase-RNase intramolecular domain interface show increased solvent exposure (Supplementary Fig. 6C). The loosening of the intramolecular interactions is consistent with the reorientation of the pIRE1 $\alpha$  dimer that leads to the dimerization of the RNase domains. Simultaneously, the decrease in overall labeling of the RNase domains occurs in concert with the conditions under which RNase domains dimerize (Fig. 5A and 5D). Third, in the presence of bound STS there is an increase in solvent exposure of the residues 900-916 (Supplementary Fig. 6D). These residues form a helix-loop element that interact directly with the RNA substrate and include the catalytically essential His910 (Korennykh et al., 2009; Dong et al., 2001). This apparent increased dynamic state of the helix-

MOL #100917

loop catalytic element may be related to the catalytic readiness favored by STS but opposed by GSK2850163.

### Comparison of pIRE1 $\alpha$ co-crystal structures

A comparison between the pIRE1 $\alpha$ -GSK2850163 and pIRE1 $\alpha$ -STS complexes shows that both structures are back-to-back dimers (Fig. 5A). Binding of GSK2850163 causes the kinase  $\alpha$ C helix (residues 610-619) to move to the inactive conformation by an average  $4.4\text{\AA} \pm 1.0\text{\AA}$  (range of  $3.03\text{\AA}$  to  $6.40\text{\AA}$  on superposition of the  $\alpha$ C helix carbon atoms) as compared with the position observed in the STS complex (Fig 5B). While the centers of mass of the kinase N-domains ( $21.5\text{\AA}$  to  $21.9\text{\AA}$ ) and C-domains ( $43.1\text{\AA}$  to  $43.6\text{\AA}$ ) remain constant, a nearly  $20^\circ$  rotation of the domains relative to one another is observed in the two structures. A differential gap of nearly  $4\text{\AA}$  between the RNase domains in the structures of pIRE1 $\alpha$ -GSK2850163 ( $29.7\text{\AA}$ ) and pIRE1 $\alpha$ -STS ( $26.1\text{\AA}$ ) is reflected in a different set of interactions across the RNase dimer interfaces. Hence, the RNase dimer interface in the pIRE1 $\alpha$ -GSK2850163 complex is reduced by 58% ( $269\text{\AA}^2$ ) compared to the pIRE1 $\alpha$ -STS complex ( $642\text{\AA}^2$ ) (Fig. 5E). In pIRE1 $\alpha$ -GSK2850163, the RNase domains are noticeably separated such that the network of interactions across the dimer is no longer possible. The interactions between the protomers of the pIRE1 $\alpha$ -GSK2850163 dimer occur mostly between the kinase domains ( $1,734\text{\AA}^2$ ), with less contact occurring between the RNase domains ( $269\text{\AA}^2$ ). This separation of RNase domains is consistent with the biochemical and cellular data showing that GSK2850163 is a potent inhibitor of pIRE1 $\alpha$  RNase activity.

In the pIRE1 $\alpha$ -STS complex, the RNase domains form a dimer with two sets of interdigitating H-bond interactions between His909, Asp847 and Arg905 ( $3.2\text{-}3.5\text{\AA}$ ), and



MOL #100917

between Arg955, Glu836, and Asp927 (3.1-3.5Å) that allow the key nuclease catalytic residues Tyr892, Arg905, Asn906, and His910 to be poised for action (Fig. 5D). Asp847, His909, Arg905 are highly conserved residues across multiple species (Dong et al., 2001). These interactions across the RNase dimer interface are also analogous to those observed previously for the activation of yeast Ire1 RNase activity by quercetin (3LJ0; Wiseman et al., 2010). In the structure of pIRE1 $\alpha$ -GSK2850163, the RNase domains are separated; thus, the network of H-bonds between the RNase domains observed in the active pIRE1 $\alpha$ +STS dimer does not exist (Fig. 5C). Hence, the data from the co-crystal structures presented here suggest that the formation of interdigitating H-bonds and the stabilization of the RNase dimer are critical for the active RNase conformation and its enzymatic activity.

MOL #100917

## DISCUSSION

Recent work has implicated the UPR in a number of diseases, most notably in cancer where UPR activation has been shown to function as a survival mechanism in cancer promoting tumor growth, regulating angiogenesis, and facilitating adaptation to hypoxia (Ma and Hendershot, 2004; Feldman et al., 2005; Chen et al., 2014). Specifically, the IRE1 $\alpha$ /XBP1 pathway has shown to be overexpressed in a variety of human cancers, and activation of the pathway has been shown to be essential for the survival of highly secretory multiple myeloma cells where the protein load is high (Koong et al., 2006; Feldman et al., 2005; Carrasco et al., 2007). These key findings, coupled with the possibility to modulate IRE1 $\alpha$  activity via targeting two potentially druggable domains, has made IRE1 $\alpha$  a very attractive target in drug discovery (Hetz et al., 2013; Maly and Papa, 2014; Harrington et al., 2014; Sanches et al., 2014; Joshi et al., 2015).

An increasing body of evidence indicates that IRE1 $\alpha$  inhibitors bound to the kinase domain invariably inhibit its ATPase activity, yet some kinase inhibitors inhibit the RNase activity while others activate its RNase activity. GSK2850163 was discovered in an attempt to identify IRE1 $\alpha$ -selective inhibitors of XBP1 splicing that could regulate multiple myeloma cancer cells. It is a highly selective kinase inhibitor; a panel of 284 kinases was assayed to determine the specificity of GSK2850163, and only two additional kinases were weakly inhibited by GSK2850163: Ron (IC<sub>50</sub> = 4.4  $\mu$ M), and FGFR1 V561M (IC<sub>50</sub> = 17  $\mu$ M) (Supplementary Table 1). GSK2850163 inhibits IRE1 $\alpha$  RNase activity due to the unique way the molecule binds in the kinase domain active site. GSK2850163 binds deep in a pocket next to the kinase  $\alpha$ C helix, approximately 12 Å from the hinge region which is clearly distinct from the

MOL #100917

ADP binding site. The molecule adopts a U-shape conformation when bound to pIRE1 $\alpha$  that could only be achieved with the *R*-stereoisomer (Supplementary Fig. 2A). Modeling of the *S*-stereoisomer places the di-fluoro benzene outside the electron density and clashes with the protein. Similarly, flipping the U-shaped molecule to the reverse orientation places the spirodecane within the electron density, but the 4-bond length between the spirodecane and the tolyl group leads to a clash with Leu616 and the 2-bond length is too short and causes a clash between the di-fluoro benzene and Lys599 instead of the H-bond when in the modeled orientation. Based on this and the SAR studies performed, it is clear that only the *R*-stereoisomer in the modeled conformation and orientation is capable of fitting the electron density, avoiding clashes, and engaging with Glu612 and Lys599.

The GSK2850163 mode of binding differs from classic ATP-competitive inhibitors (reviewed in Dar and Shokat, 2011). Inhibitors exemplified by APY29 (DFG-in and the  $\alpha$ C helix in the active conformation), activate IRE1 $\alpha$  RNase activity (Korennykh et al., 2009; Wang et al., 2012). In contrast, inhibitors like KIRA6 and several close analogs inhibit IRE1 $\alpha$  kinase and RNase activities and possibly prevent dimer association (Wang et al., 2012; Ghosh et al., 2014). While co-crystal structures for KIRA6 are not available, a close analog was recently co-crystallized with the c-Src kinase domain demonstrating a shift in the  $\alpha$ C-helix 'out' to the inactive conformation (PDB ID [3QLF](#)). Thus, it is possible that KIRA6 invokes a similar conformational change when bound to IRE1 $\alpha$ . Similarly, another inhibitor recently described by Amgen potently inhibited IRE1 $\alpha$  kinase and RNase activity and was co-crystallized with a dephosphorylated IRE $\alpha$  monomer (Harrington et al., 2014). The lack of IRE1 $\alpha$  dimer structure here could be due to the compound either preventing dimerization or stabilizing a monomeric form of IRE1 $\alpha$ . While previously it was suggested that dimerization/oligomerization occurs after

MOL #100917

autophosphorylation, recent crystal structures of dephosphorylated human IRE1 $\alpha$  dimers demonstrate that dimerization can precede phosphorylation in both “face-to-face” and “back-to-back” configurations (Ali et al., 2011; Joshi et al., 2015). It should also be noted that this molecule shifted the  $\alpha$ C-helix ‘out.’ Hence, one commonality between this molecule, GSK2850163, and the KIRA6 analogs, is that all these inhibitors shift the  $\alpha$ C-helix to an inactive conformation which may likely be a requirement for IRE1 $\alpha$  RNase inactivation.

Aside from kinase domain inhibitors, two other classes of IRE1 $\alpha$  inhibitors have been characterized that target other potential drug pockets in the IRE1 $\alpha$  protein: quercetin and salicylaldehyde-based inhibitors. Quercetin binds uniquely to yeast Ire1 in a pocket at the enzyme-dimer interface termed the Q-site, thereby stabilizing Ire1 in an active conformation that augments RNase activity (Wiseman et al., 2010). While quercetin has been shown to be a broad spectrum kinase inhibitor and may potentially target the nucleotide binding site of Ire1, it did not inhibit Ire1 autophosphorylation. Independently, a considerable amount of work has been conducted to target IRE1 $\alpha$  RNase activity directly (Maly and Papa, 2014; Sanches et al., 2014). These salicylaldehyde-based inhibitors contain a reactive electrophile that most likely covalently modifies Lys907 at the IRE1 $\alpha$  RNase active site. It is believed that these inhibitors should not affect IRE1 $\alpha$  autophosphorylation or dimerization. GSK2850163 is the first molecule that inhibits both kinase and RNase activity by binding to phosphorylated IRE1 $\alpha$  and inducing a unique long-range conformation change which alters the preferred enzyme structure for RNA substrate binding.

The wealth of data on the dimeric/oligomeric state of IRE1 as a function of phosphorylation and the effects of various classes of kinase inhibitors does not fully explain the

MOL #100917

details of the conformational changes required to cause modulation of IRE1 $\alpha$  RNase activity. The hydrogen-deuterium exchange (HDX) rate, which is dependent on both structural and conformational changes, is very well suited to reveal these details and has the resolution necessary to pinpoint the required conformational changes in solution state. Our HDX data is consistent with the model of RNase inhibition suggested by the pIRE1 $\alpha$ -GSK2850163 co-crystal structure. The differences observed in labeling overlap with the changes observed in the crystal state. The critical observation of the conserved salt bridge between Arg627 and Asp620 in the kinase domain being disrupted by GSK2850163 is highly consistent with the changes in the  $\alpha$ C helix to the 'out' (inactive) conformation and the reorientation of the pIRE1 $\alpha$  dimer to the inactive form. By the same analysis, the reverse is true in the activation of the RNase.

A comparison of the yeast Ire1 "back to back" dimers with the human pIRE1 $\alpha$ -STS dimer demonstrates that the kinase domain DFG-loop is in the "in" conformation, the  $\alpha$ C helix is in the active conformation, and the RNase domains are engaged through a network of H-bond interactions in these structures that coincide with conditions of RNase activation. Minor differences are observed between the pIRE1 $\alpha$ -STS dimer and the three yeast Ire1 structures (PDB IDs [2RIO](#); [3FBV](#); [3LJ0](#)) (r.m.s. on C $\alpha$  = 1.9-2.1Å); however, differences are even greater when comparisons are made with the pIRE1 $\alpha$ -GSK2850163 dimer (r.m.s. on C $\alpha$  = 3.3-3.4Å). GSK2850163 binding results in shifting the structure of the kinase domain to the DFG-out,  $\alpha$ C helix inactive conformation, and the RNase domains of the dimer are rotated away from each other. This indicates that the RNase active forms of yeast and human IRE1 are markedly different from the RNase inactive pIRE1 $\alpha$ -GSK2850163 dimer. While the key interactions in the RNase domains are not mediated by identical residues across species, they are essential.

MOL #100917

Mutagenesis studies have shown that these interfacial residues are critical for maintaining RNase activity (Lee et al., 2008).

Structural similarities are also observed between the human phosphorylated (4YZD) and dephosphorylated (3P23) IRE1 $\alpha$ -ADP-Mg<sup>2+</sup> structures (r.m.s. on C $\alpha$  = 0.5Å). In both cases, the dimers are “face-to-face” with the RNase domains separated in an inactive conformation. Likewise, pIRE1 $\alpha$ -ADP-Mg<sup>2+</sup> and mouse IRE1 complexed with the RNase domain inhibitor, MKC9989, (4PL3) are similar in dimeric structure (r.m.s on C $\alpha$  = 0.8Å). The largest differences are located in a loop formed by residues 654-659 in the kinase domain. This stretch of amino acids is engaged in intermolecular contacts within the neighboring molecule of the asymmetric unit in the ADP complex. It is worth noting that previous *in vitro* studies have shown that ADP bound to IRE1 $\alpha$  can affect dimerization and/or reduce RNase activity of both mouse and human IRE1 $\alpha$  (Prischi et al., 2014; Sanches et al., 2014).

The pIRE1 $\alpha$ -GSK2850163 and pIRE1 $\alpha$ -STS co-crystal structures were also compared to two recently reported human “back-to-back” dimers of IRE1 $\alpha$ : one in apo form (4Z7G) and one in an inhibitor-bound form (4Z7H). In these two structures, the RNase domains are not engaging with each other across the dimer interface and more closely resemble the pIRE1 $\alpha$ +GSK2850163 dimer (overall dimer r.m.s. on C $\alpha$  = 1.6Å) than the pIRE1 $\alpha$ +STS dimer (overall dimer r.m.s. on C $\alpha$  = 2.7Å). Despite this, the imidazopyridine molecule, compound 3, interacts with the hinge and the activation loop (DFG-in) in a similar fashion as staurosporine (r.m.s. on C $\alpha$  = 0.9Å) and behaves as a type I kinase inhibitor (Joshi et al., 2015). GSK2850163 and compound 3 do not occupy overlapping pockets. This structural observation is at odds with other type I inhibitor bound IRE1 structures. A comparison of the IRE1 $\alpha$  apo and IRE1 $\alpha$ -imidazopyridine complex

MOL #100917

indicates that they are nearly identical (r.m.s. on Ca = 0.6Å). This discrepancy may be due to the way the experiments were performed, namely that the inhibitor-bound form was resolved by soaking into the pre-formed apo crystals as opposed to performing co-crystallization.

The characterization of the first co-crystal structure of human phosphorylated IRE1 $\alpha$  and its complex with a new class of kinase inhibitor has revealed a novel mode of action for the inhibition of pIRE1 $\alpha$  kinase and RNase activity. The comparisons made between known structures across various species and with inhibitors that have differential effects on IRE1 $\alpha$  RNase activity should provide insights into the molecular mechanisms responsible for activation and inhibition of IRE1 $\alpha$  RNase activity. These new data should also provide a feasible path to enable the design and use of pharmacological agents that differentially affect IRE1 $\alpha$ /XBP1 signaling.

Coordinates for the pIRE1 $\alpha$ +GSK2350163, pIRE1 $\alpha$ +ADP, and pIRE1 $\alpha$ +STS co-crystal structures have been deposited to the Protein Data Bank with the respective accession codes: PDB ID 4YZ9, 4YZD, and 4YZC.

MOL #100917

## **ACKNOWLEDGEMENTS**

We would like to thank the members of the IRE1 $\alpha$  drug discovery program and the Computational and Structural Chemistry Department for fruitful discussions and insightful comments on the manuscript.

## **AUTHOR CONTRIBUTIONS**

*Participated in research design:* Evans, Heerding, Buser, Su, DeYoung

*Conducted experiments:* Concha, Smallwood, Bonnette, Totoritis, Federowicz, Campobasso, Choudhry, Shuster, Evans, Su, DeYoung

*Contributed new reagents or analytic tools:* Qi, Chen, Sweitzer, Shuster, Evans, Ralph

*Performed data analysis:* Concha, Smallwood, Totoritis, Zhang, Yang, Choudhry, Heerding, Su, DeYoung

*Wrote or contributed to the writing of the manuscript:* Concha, Buser, Su, DeYoung



MOL #100917

## REFERENCES

- Ali MM, Bagratuni T, Davenport EL, Nowak PR, Silva-Santisteban MC, Hardcastle A, McAndrews C, Rowlands MG, Morgan GJ, and Aherne W et al. (2011) Structure of the Ire1 autophosphorylation complex and implications for the unfolded protein response. *EMBO J* **30**:894-905.
- Afonine PV, Mustyakimov M, Grosse-Kunstleve RW, Moriarty NW, Langan P, and Adams PD (2010) Joint X-ray and neutron refinement with phenix.refine. *Acta Cryst D Biol Crystallogr* **66**:1153-1163.
- Bagratuni T, Wu P, Gonzalez de Castro D, Davenport EL, Dickens NJ, Walker BA, Boyd K, Johnson DC, Gregory W, and Morgan GJ et al. (2010) XBP1s levels are implicated in the biology and outcome of myeloma mediating different clinical outcomes to thalidomide-based treatments. *Blood* **116**:250-253.
- Calfon M, Zeng H, Urano F, Till JH, Hubbard SR, Harding HP, Clark SG, and Ron D (2002) IRE1 couples endoplasmic reticulum load to secretory capacity by processing the XBP-1 mRNA. *Nature* **415**:92-96.
- Carrasco DR, Sukhdeo K, Protopopova M, Sinha R, Enos M, Carrasco DE, Zheng M, Mani M, Henderson J, and Pinkus GS et al. (2007) The differentiation and stress response factor XBP-1 drives multiple myeloma pathogenesis. *Cancer Cell* **11**:349-360.
- Chen VB, Arendall WB 3rd, Headd JJ, Keedy DA, Immormino RM, Kapral GJ, Murray LW, Richardson JS, and Richardson DC (2010) MolProbity: all-atom structure validation for macromolecular crystallography. *Acta Cryst D Biol Crystallogr* **66**:12-21.
- Chen X, Iliopoulos D, Zhang Q, Tang Q, Greenblatt MB, Hatziapostolou M, Lim E, Tam WL, Ni M, and Chen Y et al. (2014) XBP1 promotes triple-negative breast cancer by controlling the HIF1 $\alpha$  pathway. *Nature* **508**:103-107.
- Cross BC, Bond PJ, Sadowski PG, Jha BK, Zak J, Goodman JM, Silverman RH, Neubert TA, Baxendale IR, and Ron D et al. (2012) The molecular basis for selective inhibition of unconventional mRNA splicing by an IRE1-binding small molecule. *Proc Natl Acad Sci USA* **109**:E869-E878.
- Dar AC and Shokat KM (2011) The evolution of protein kinase inhibitors from antagonists to agonists of cellular signaling. *Annu Rev Biochem* **80**:769-795.
- Dong B, Niwa M, Walter P, and Silverman RH (2001) Basis for regulated RNA cleavage by functional analysis of RNase L and Ire1p. *RNA* **7**:361-373.
- Emsley PP and Cowtan K (2004) Features and development of Coot. *Acta Cryst D Biol Crystallogr* **66**:486-501.

MOL #100917

- Englander JJ, Del Mar C, Li W, Englander SW, Kim JS, Stranz DD, Hamuro Y, and Woods VL Jr. (2003) Protein structure change studied by hydrogen-deuterium exchange, functional labeling, and mass spectrometry. *Proc Natl Acad Sci USA* **100**:7057-7062.
- Feldman DE, Chauhan V, and Koong AC (2005) The unfolded protein response: a novel component of the hypoxic stress response in tumors. *Mol Cancer Res* **3**:597-605.
- Ghosh R, Wang L, Wang ES, Perera BG, Igbaria A, Morita S, Prado K, Thamsen M, Caswell D, and Macias H et al. (2014) Allosteric inhibition of the IRE1 $\alpha$  RNase preserves cell viability and function during endoplasmic reticulum stress. *Cell* **158**:534-548.
- Harding HP, Calton M, Urano F, Novoa I, and Ron D (2002) Transcriptional and translational control in the mammalian unfolded protein response. *Annu Rev Cell Dev Biol* **18**:575-599.
- Harrington PE, Biswas K, Malwitz D, Tasker AS, Mohr C, Andrews KL, Dellamaggiore K, Kendall R, Beckmann H, and Jaekel P et al. (2014) Unfolded Protein Response in Cancer: IRE1 $\alpha$  Inhibition by Selective Kinase Ligands Does Not Impair Tumor Cell Viability. *ACS Med Chem Lett* **6**:68-72.
- Hetz C, Chevet E, and Harding HP (2013) Targeting the unfolded protein response in disease. *Nat Rev Drug Discov* **12**:703-719.
- Hollien J and Weissman JS (2006) Decay of endoplasmic reticulum-localized mRNAs during the unfolded protein response. *Science* **313**:104-107.
- Joshi A, Newbatt Y, McAndrew PC, Stubbs M, Burke R, Richards MW, Bhatia C, Caldwell JJ, McHardy T, and Collins I et al. (2015) Molecular mechanisms of human IRE1 activation through dimerization and ligand binding. *Oncotarget* Apr 18. [Epub ahead of print].
- Koong AC, Chauhan V, and Romero-Ramirez L (2006) Targeting XBP-1 as a novel anti-cancer strategy. *Cancer Biol Ther* **5**:756-759.
- Korennykh AV, Egea PF, Korostelev AA, Finer-Moore J, Zhang C, Shokat KM, Stroud RM, and Walter P (2009) The unfolded protein response signals through highorder assembly of Ire1. *Nature* **457**:687-693.
- Kornev AP and Taylor SS (2010) Defining the conserved internal architecture of a protein kinase. *Biochim Biophys Acta* **1804**:440-444.
- Lee AH, Iwakoshi NN, and Glimcher LH (2003) XBP-1 regulates a subset of endoplasmic reticulum resident chaperone genes in the unfolded protein response. *Mol Cell Biol* **23**:7448-7459.
- Lee K, Tirasophon W, Shen X, Michalak M, Prywes R, Okada T, Yoshida H, Mori K, and Kaufman RJ (2002) IRE1-mediated unconventional mRNA splicing and S2P-mediated ATF6 cleavage merge to regulate XBP1 in signaling the unfolded protein response. *Genes Dev* **16**:452-466.

MOL #100917

- Lee KP, Dey M, Neculai D, Cao C, Dever TE, and Sicheri F (2008) Structure of the dual enzyme Ire1 reveals the basis for catalysis and regulation in nonconventional RNA splicing. *Cell* **132**:89-100.
- Ma Y and Hendershot LM (2004) The role of the unfolded protein response in tumor development: friend or foe?. *Nat Rev Cancer* **4**:966-977.
- Maly DJ and Papa FR (2004) Druggable sensors of the unfolded protein response. *Nat Chem Biol* **10**:892-901.
- Murshudov GNG, Vagin AA, and Dodson EJ (1997) Refinement of macromolecular structures by the maximum-likelihood method. *Acta Cryst D Biol Crystallogr* **53**:240-255.
- Nakamura M, Gotoh T, Okuno Y, Tatetsu H, Sonoki T, Uneda S, Mori M, Mitsuya H, and Hata H (2006) Activation of the endoplasmic reticulum stress pathway is associated with survival of myeloma cells. *Leuk Lymphoma* **47**:531-539.
- Percy AJ, Rey M, Burns KM, and Shriemer DC (2012) Probing protein interactions with hydrogen/deuterium exchange and mass spectrometry—a review. *Anal Chim Acta* **721**:7-21.
- Prischi F, Nowak PR, Carrara M, and Ali MM (2014) Phosphoregulation of Ire1 RNase splicing activity. *Nat Commun* **5**:doi: 10.1038/ncomms4554.
- Reimold AM, Iwakoshi NN, Manis J, Vallabhajosyula P, Szomolanyi-Tsuda E, Gravalles EM, Friend D, Grusby MJ, Alt F, and Glimcher LH (2001) Plasma cell differentiation requires the transcription factor XBP-1. *Nature* **412**:300-307.
- Ron D (2002) Translational control in the endoplasmic reticulum stress response. *J Clin Invest* **110**:1383-1388.
- Rouschop KM, van den Beuken T, Dubois L, Niessen H, Bussink J, Savelkoul K, Keulers T, Mujcic H, Landuyt W, and Voncken JW, et al. (2010) The unfolded protein response protects human tumor cells during hypoxia through regulation of the autophagy genes MAP1LC3B and ATG5. *J Clin Invest* **120**:127-141.
- Sanches M, Duffy NM, Talukdar M, Thevakumaran N, Chiovitti D, Canny MD, Lee K, Kurinov I, Uehling D, and Al-awar R et al. (2014) Structure and mechanism of action of the hydroxy-aryl-aldehyde class of IRE1 endoribonuclease inhibitors. *Nat Commun* **5**:doi: 10.1038/ncomms5202.
- Schroder M and Kaufman RJ (2005) The mammalian unfolded protein response. *Annu Rev Biochem* **74**:739-789.
- Tirasophon W, Welihinda AA, and Kaufman RJ (1998) A stress response pathway from the endoplasmic reticulum to the nucleus requires a novel bifunctional protein kinase/endoribonuclease (Ire1p) in mammalian cells. *Genes Dev* **12**:1812-1824.

MOL #100917

- Urano F, Wang X, Bertolotti A, Zhang Y, Chung P, Harding HP, and Ron D (2000) Coupling of stress in the ER to activation of JNK protein kinases by transmembrane protein kinase IRE1. *Science* **287**:664-666.
- Walter P and Ron D (2011) The unfolded protein response: from stress pathway to homeostatic regulation. *Science* **334**:1081-1086.
- Wang L, Perera BG, Hari SB, Bhatarai B, Backes BJ, Seeliger MA, Schürer SC, Oakes SA, Papa FR, and Maly DJ (2012) Divergent allosteric control of the IRE1alpha endoribonuclease using kinase inhibitors. *Nat Chem Biol* **8**:982-989.
- Wang Y, Shen J, Arenzana N, Tirasophon W, Kaufman RJ, and Prywes R (2000) Activation of ATF6 and an ATF6 DNA binding site by the endoplasmic reticulum stress response. *J Biol Chem* **275**:27013-27020.
- Wasilko DJ and Lee SE (2006) TIPS: Titerless Infected-Cells Preservation and Scale-Up. *BioProc J* **5**:29-32.
- Winn MD, Ballard CC, Cowtan KD, Dodson EJ, Emsley P, Evans PR, Keegan RM, Krissinel EB, Leslie AG, and McCoy A (2011) Overview of the CCP4 suite and current developments. *Acta Cryst D Biol Crystallogr* **67**:235-242.
- Wiseman RL, Zhang Y, Lee KP, Harding HP, Haynes CM, Price J, Sicheri F, and Ron D (2010) Flavonol activation defines an unanticipated ligand-binding site in the kinase-RNase domain of IRE1. *Mol Cell* **38**:291-304.
- Woehlbier U and Hetz C (2011) Modulating stress responses by the UPRosome: A matter of life and death. *Trends Biochem Sci* **36**:329-337.
- Yoshida H, Matsui T, Yamamoto A, Okada T, and Mori K (2001) XBP1 mRNA is induced by ATF6 and spliced by IRE1 in response to ER stress to produce a highly active transcription factor. *Cell* **107**:881-891.

MOL #100917

## FOOTNOTES

All authors are past or present employees of GlaxoSmithKline. No potential conflicts of interest were disclosed by the authors.

MOL #100917

## FIGURE LEGENDS

**Fig. 1.** GSK2850163 binds to human pIRE1 $\alpha$  and inhibits XBP1 splicing. (A) GSK2850163 is a selective inhibitor of pIRE1 $\alpha$  kinase activity and RNase activity. It exhibits no or weak inhibition towards a wide range of the other kinases (shown here is the UPR kinase, PERK) and nucleases (shown here is RNase L, its closest homolog). Refer to *Materials and Methods* for assay details. (B) Overall structure of the pIRE1 $\alpha$ -GSK2850163 (PDB ID: 4YZ9) back-to-back dimer. Inset: chemical structure of GSK2850163 ((R)-2-(3,4-dichlorobenzyl)-N-(4-methylbenzyl)-2,7-diazaspiro[4.5]decane-7-carboxamide). (C) GSK2850163 (yellow) binds next to the  $\alpha$ C helix and displaces the activation loop (DFG-out) such that it is occupying the ATP-binding site represented by its surface. GSK2850163 makes H-bond interactions with key kinase catalytic residues Lys599 (K599) and Glu612 (E612). (D) For comparison, the DFG loop is in the “in” conformation in the structure of pIRE1 $\alpha$ -Mg<sup>2+</sup>-ADP (PDB ID: 4YZD), and Phe712 (F712) occupies the same pocket where the GSK2850163 would bind. For both (C) and (D), the asterisk (\*) indicates the C-terminal end of the visible portion of the activation loop.

**Fig. 2.** Selected SAR results of compound **1** (GSK2850163). (A). Replacement of the urea nitrogen with a carbon atom (compound **2**) or capping the NH with a methyl group (compound **3**) caused a loss of potency. Conversion of basic amine in pyrrolidine ring to a non basic amide yielded an inactive analog (compound **4**). (B and C). The lipophilic groups at the tolyl and dichlorophenyl groups were critical for the compound’s activity. On the other hand, the polar functionalities, such as pyridines, were not tolerated.

**Fig. 3.** Inhibition of IRE1 $\alpha$  kinase and RNase activity in cells treated with GSK2850163. (A) Multiple myeloma cell lines were left untreated or treated with tunicamycin for 1 hour.

MOL #100917

GSK2850163 (GSK163) was then added for 3 hours at the indicated doses. Total RNA was harvested and RT-PCR was performed using human-specific XBP1 primers flanking the splice site that distinguish between unspliced (XBP1<sub>u</sub>) and spliced (XBP1<sub>s</sub>) XBP1 mRNA. (B) RPMI 8226 cells were left untreated or treated with tunicamycin and/or GSK2850163 as described in (A). Changes in IRE1 $\alpha$  phosphorylation were detected by western blot using a phospho-specific antibody raised against Ser 724 in the kinase activation loop. (C) XBP1s transcriptional activity is reduced in cells treated with GSK2850163. PANC-1 cells were transfected with a 5X UPRE luciferase reporter and pRL-SV40 renilla constructs. 48 hours later, cells were left untreated or treated with tunicamycin for 1 hour, followed by GSK2850163 treatment for 16 hours. UPRE luciferase expression was measured and normalized to renilla expression levels.

**Fig. 4.** Structure and activity of the human pIRE1 $\alpha$ -STS (STS) complex. (A) STS inhibits pIRE1 $\alpha$  kinase activity but not RNase activity. (B) Titration curve showing that the nuclease activity of dephosphorylated IRE1 $\alpha$  (IRE1 $\alpha$  (-P)) is stimulated by STS in the RNase assay. (C) STS induces XBP1 splicing in RPMI 8826 cells. Cells were treated with STS for 30 minutes, followed by tunicamycin (tuni, 5 $\mu$ g/mL) treatment in half of the cells for 1 hour. Total RNA was harvested and RT-PCR was performed using human-specific XBP1 primers flanking the splice site that distinguish between unspliced (XBP1<sub>u</sub>) and spliced (XBP1<sub>s</sub>) XBP1 mRNA. (D) STS inhibits tunicamycin-induced IRE1 $\alpha$  phosphorylation. RPMI 8226 cells were treated as described in (c). Changes in IRE1 $\alpha$  phosphorylation were detected by western blot using a phospho-specific antibody raised against Ser 724 in the kinase activation loop. (E) pIRE1 $\alpha$ -STS dimer (PDB ID: 4YZC) in the back-to-back configuration with STS bound in the ATP-binding site.

MOL #100917

**Fig. 5.** Conformational changes to pIRE1 $\alpha$  upon ligand binding. (A) Left panel, increased interactions along the kinase dimer interface and decreased surface area contact of the RNase domains in pIRE1 $\alpha$  + GSK2850163; Right panel, pIRE1 $\alpha$ -STS structure where the interactions are tighter between the RNase domains. A cartoon model depicts a rocking motion between inactive (left) and active (right) pIRE1 $\alpha$  dimers. (B) Residues 610-619 that make up the  $\alpha$ C helix move  $4.4 \text{ \AA} \pm 1.0$  between pIRE1 $\alpha$ -STS (green) and pIRE1 $\alpha$ -GSK2850163 (salmon). The structures of the kinase domains were superimposed using C $\alpha$  atoms of the residues forming the hinge region. (C) Bottom-up view of the pIRE1 $\alpha$ -GSK2850163 RNase domains. There is one pair of residues interacting across the RNase dimer interface which covers a contact area of  $269 \text{ \AA}^2$ . Glu913 on chain A (green) and Arg905 on chain B (cyan) form a salt bridge, but the equivalent interaction (i.e., Glu913 of chain B and Arg905 of chain A) is not possible because the side chain of Glu913 in chain B is disordered. (D) Bottom-up view of the pIRE1 $\alpha$ -STS RNase domains. There are two sets of interdigitating H-bond interactions, the first set involves His909, Asp847 and Arg905 (3.2-3.5 $\text{\AA}$ ), and the second is between Arg955, Glu836, and Asp927 (3.1-3.5 $\text{\AA}$ ). (E) Calculated buried surface area of contact for the two pIRE1 $\alpha$  dimers and the individual domains.

(Data Supplement 1) Crystal Structure of human phosphorylated IRE1 alpha in complex with a type III kinase inhibitor (GSK2850163A) (PDB ID: 4YZ9).

(Data Supplement 2) Crystal Structure of human phosphorylated IRE1 alpha in complex with ADP- Mg<sup>2+</sup> (PDB ID: 4YZD).

(Data Supplement 3) Crystal structure of pIRE1 alpha in complex with staurosporine (PDB ID: 4YZC).



MOL #100917

## TABLES

**Table 1. Data collection and refinement statistics (molecular replacement)**

	pIRE1 $\alpha$ +GSK2850163	pIRE1 $\alpha$ + ADP	pIRE1 $\alpha$ + STS
<b>Data collection</b>			
Space group	<i>P2<sub>1</sub>2<sub>1</sub>2</i>	<i>C2</i>	<i>P2<sub>1</sub>2<sub>1</sub>2<sub>1</sub></i>
Cell dimensions			
<i>a, b, c</i> (Å)	244.0, 77.8, 88.3	191.8, 122.5, 77.9	49.3, 155.3, 155.6
$\alpha, \beta, \gamma$ (°)	90, 90, 90	90.0, 107.1, 90.0	90, 90, 90
Molecules/a.u.	3	3	2
Resolution (Å)	2.45 ( 2.54 – 2.45)	3.14 (3.25 – 3.10)	2.62 (2.71 – 2.62)
<i>R</i> <sub>sym</sub> or <i>R</i> <sub>merge</sub>	0.073 (0.592)	0.087 (0.569)	0.118 (0.565)
<i>I</i> / $\sigma$ <i>I</i>	22.9 (3.1)	15.2 (2.4)	22.7 (5.6)
Completeness (%)	96.7 (89.7)	100.0 (100.0)	100.0 (100.0)
Redundancy	6.3 (6.3)	3.8 (3.8)	11.8 (11.6)
<b>Refinement</b>			
Resolution (Å)	30.0 – 2.45	45.6 – 3.14	40.0 – 2.62
No. reflections	59,654	60,654	41,900
<i>R</i> <sub>work</sub> / <i>R</i> <sub>free</sub>	0.24/0.29	0.20/0.25	0.25/0.29
No. atoms			
Protein	17,853	9,822	12,041
Ligand/ion	90	90	70
Water	81	35	62
<i>B</i> -factors			
Protein	57	31	55
Ligand/ion	57	24	23
Water	51	10	48
R.m.s. deviations			
Bond lengths (Å)	0.007	0.008	0.002
Bond angles (°)	0.93	1.09	1.15

Note: Values in parentheses are for highest-resolution shell.

Each dataset was collected from a single crystal

**Figure 1.**

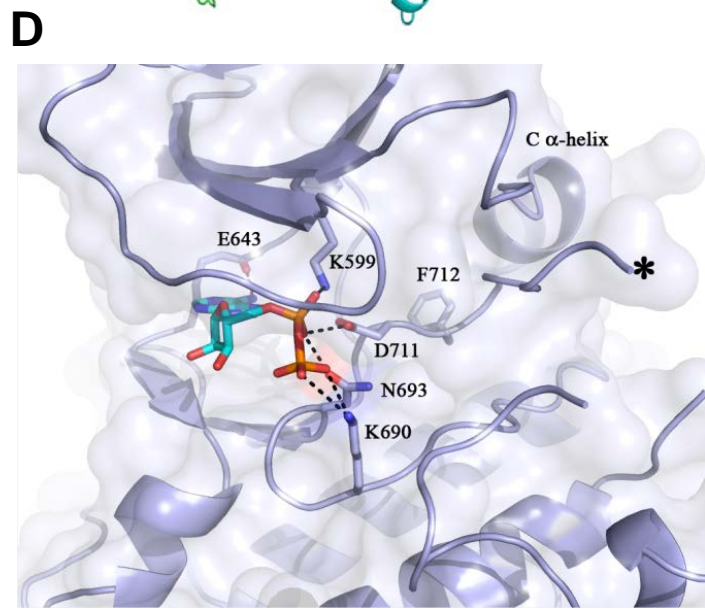
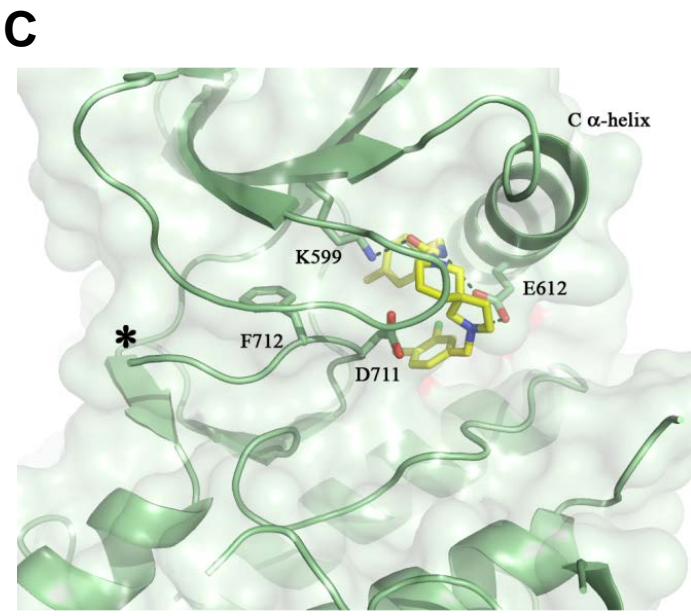
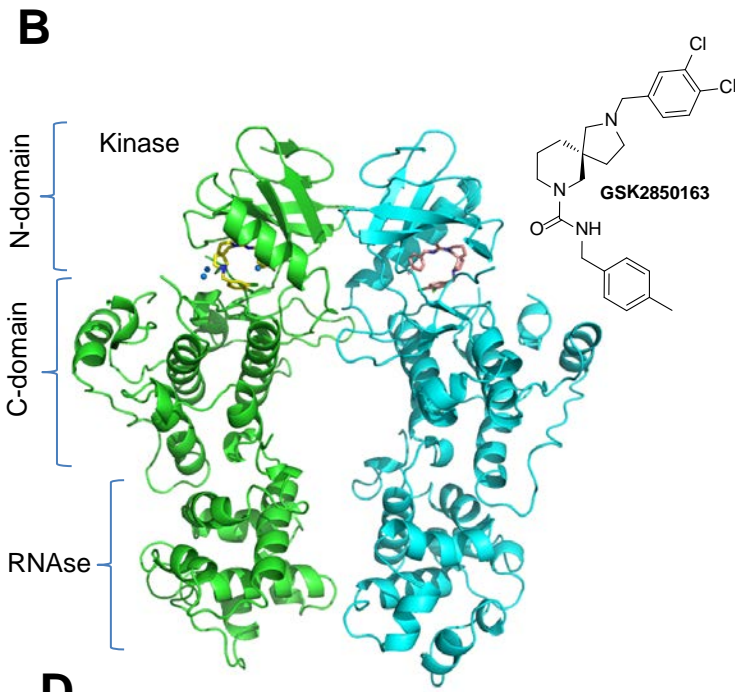
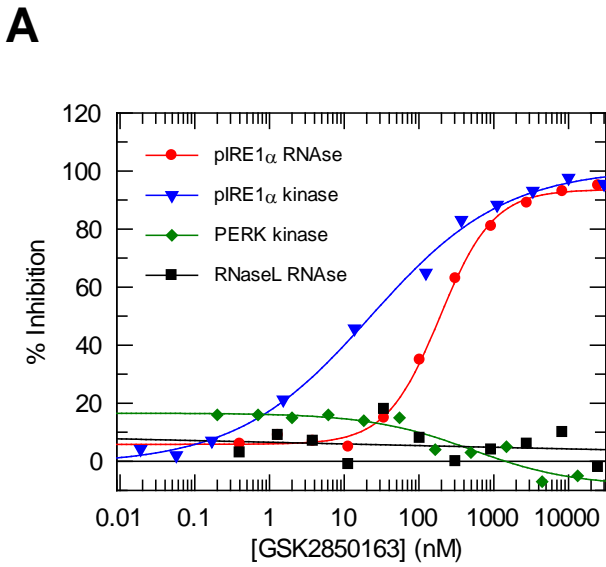
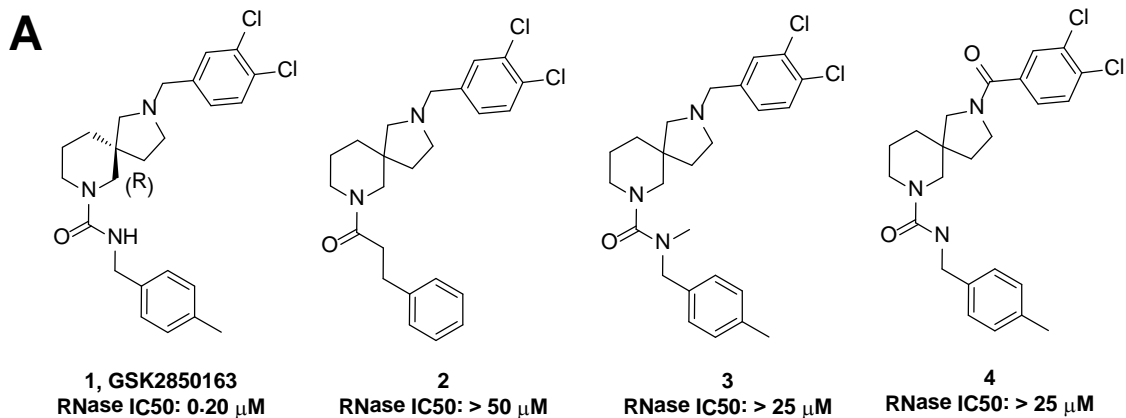
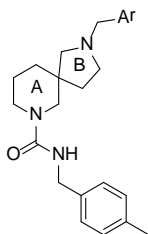


**Figure 2.**



**B**

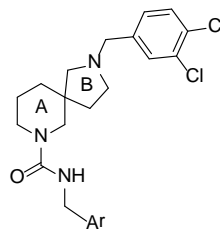
SAR Results of B-ring Aryl group



Comp #	Ar	RNase IC <sub>50</sub> (μM)
1	3,4-diClPh	0.20
5	4-Me-3-pyridyl	>25
6	4-Cl-2-pyridyl	>25
7	3-ClPh	10
8	4-ClPh	0.40
9	4-MePh	1.0
10	4-CF <sub>3</sub> Ph	0.32
11	4-Cl, 3-FPh	0.25
12	4-Cl, 3-MePh	0.32
13	4-Cl, 3-OMePh	0.20
14	4-Cl, 3-CF <sub>3</sub> Ph	10

**C**

SAR Results of A-ring Aryl group



Comp #	Ar	RNase IC <sub>50</sub> (μM)
1	4-MePh	0.20
15	4-pyridyl	6.3
16	3-pyridyl	7.9
17	2-pyridyl	12.5
18	4-Me-3-pyridyl	12.5
19	4-Me-2-pyridyl	10
20	Ph	0.40
21	4-ClPh	0.50
22	4-OMePh	0.50
23	4-F Ph	0.79
24		0.1

**Figure 3.**

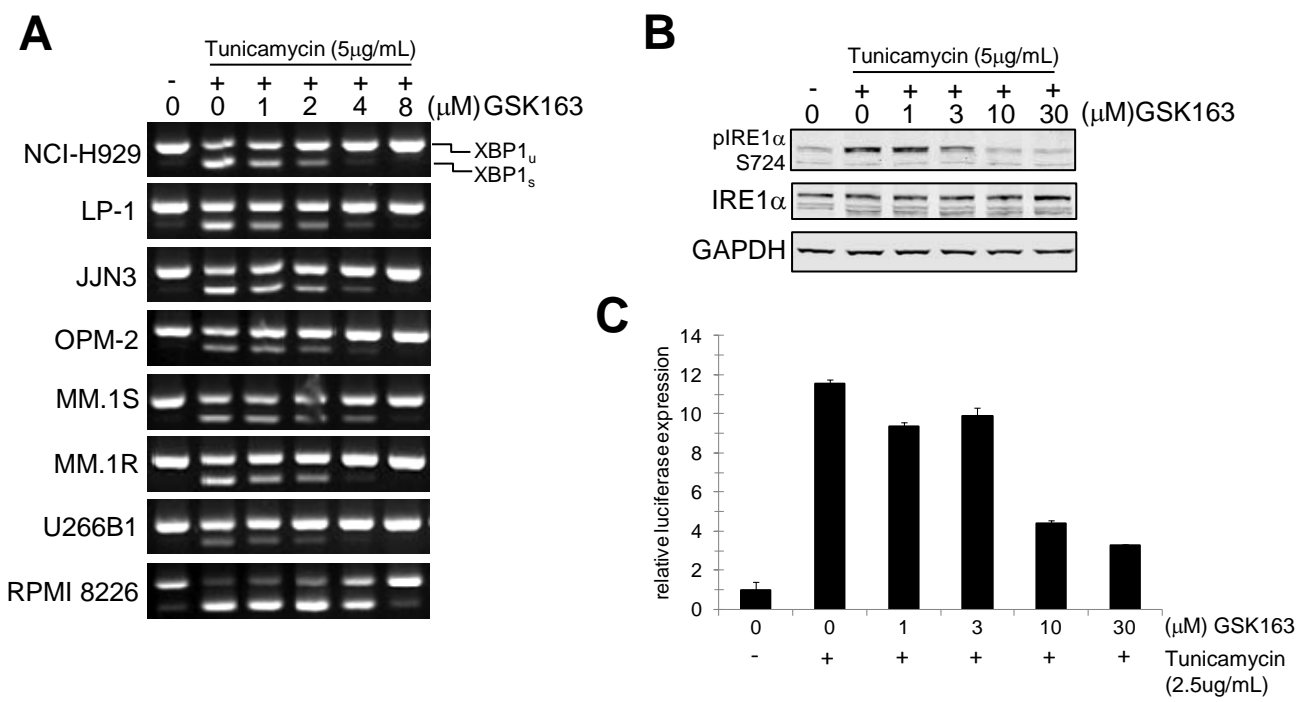


**Figure 4.**

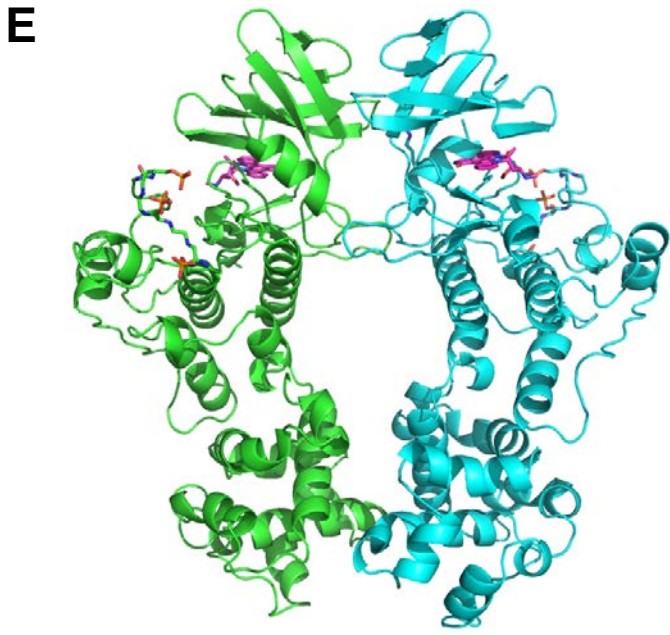
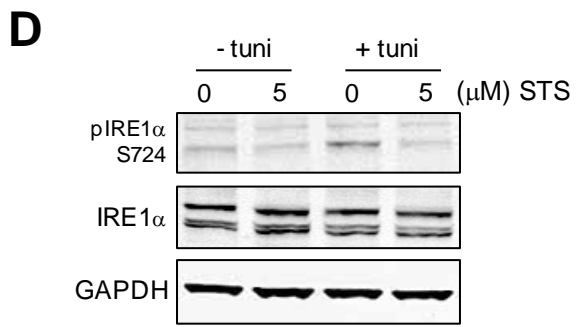
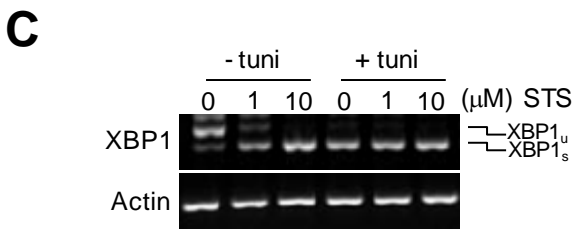
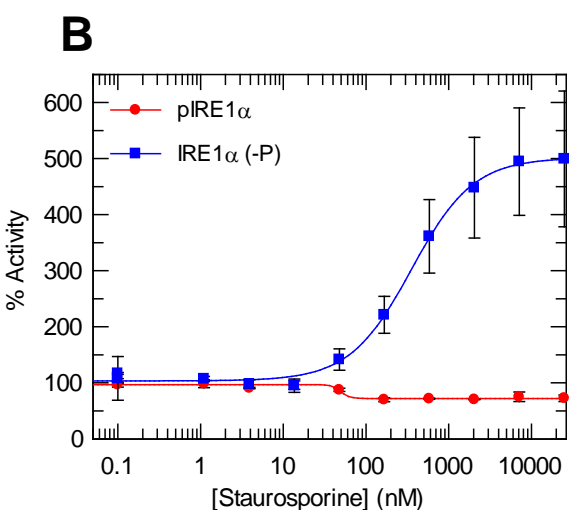
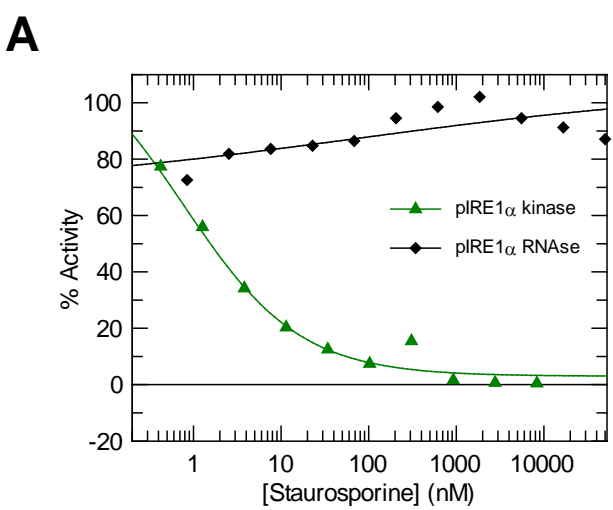
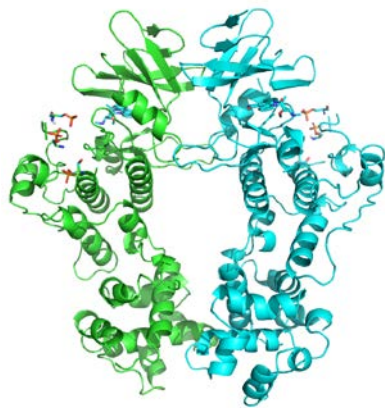


**Figure 5.**

**A**

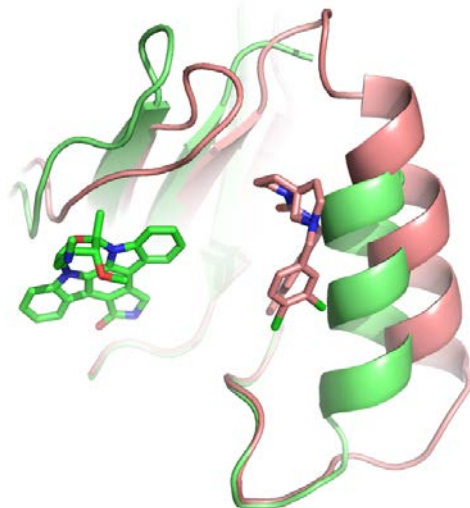


pIRE1 $\alpha$ -GSK2850163

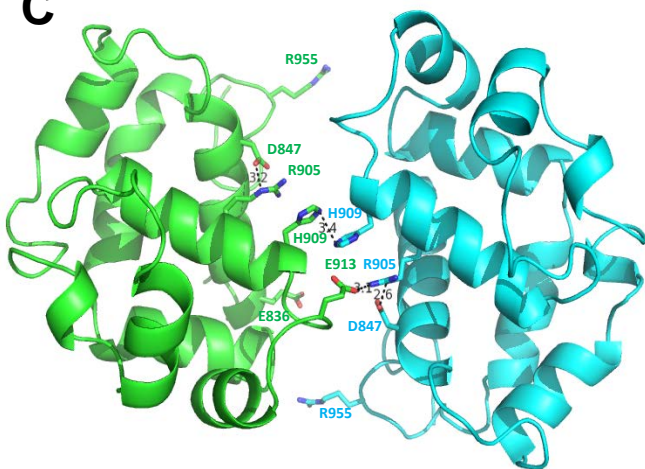


pIRE1 $\alpha$ -STC

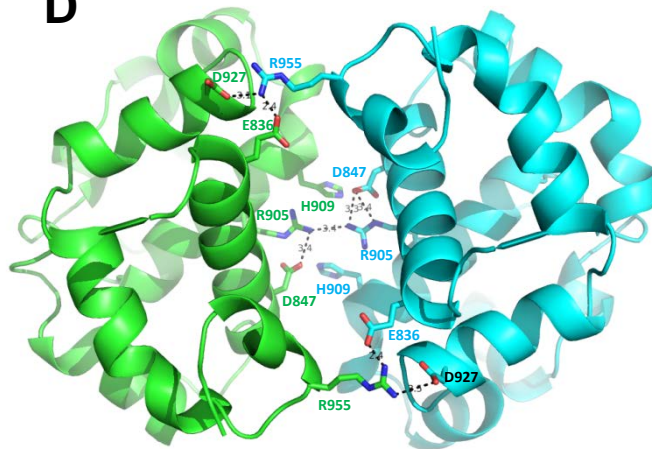
**B**



**C**



**D**



**E**

	Surface area of contact	
	GSK2850163	STC
Kinase domain	1,734 Å <sup>2</sup>	1,461 Å <sup>2</sup>
RNase domain	269 Å <sup>2</sup>	642 Å <sup>2</sup>
Dimer	2,003 Å <sup>2</sup>	2,103 Å <sup>2</sup>